IOP PUBLISHING NANOTECHNOLOGY
Nanotechnology **18** (2007) 165303 (8pp) doi:10.1088/0957-4484/18/16/165303

A micromachined membrane-based active probe for biomolecular mechanics measurement

H Torun[1], J Sutanto[1,4], K K Sarangapani[1], P Joseph[2], F L Degertekin[1] and C Zhu[1,3]

[1] GWW School of Mechanical Engineering, Georgia Institute of Technology, USA
[2] Microelectronic Research Center, Georgia Institute of Technology, USA
[3] Wallace H Coulter Department of Biomedical Engineering, Georgia Institute of Technology, USA

E-mail: levent@gatech.edu (F L Degertekin)

Received 7 December 2006, in final form 9 February 2007
Published 23 March 2007
Online at stacks.iop.org/Nano/18/165303

Abstract
A novel micromachined, membrane-based probe has been developed and fabricated as assays to enable parallel measurements. Each probe in the array can be individually actuated, and the membrane displacement can be measured with high resolution using an integrated diffraction-based optical interferometer. To illustrate its application in single-molecule mechanics experiments, this membrane probe was used to measure unbinding forces between L-selectin reconstituted in a polymer-cushioned lipid bilayer on the probe membrane and an antibody adsorbed on an atomic force microscope cantilever. Piconewton range forces between single pairs of interacting molecules were measured from the cantilever bending while using the membrane probe as an actuator. The integrated diffraction-based optical interferometer of the probe was demonstrated to have <10 fm $\mathrm{Hz}^{-1/2}$ noise floor for frequencies as low as 3 Hz with a differential readout scheme. With soft probe membranes, this low noise level would be suitable for direct force measurements without the need for a cantilever. Furthermore, the probe membranes were shown to have 0.5 μm actuation range with a flat response up to 100 kHz, enabling measurements at fast speeds.

(Some figures in this article are in colour only in the electronic version)

1. Introduction

Applications of atomic force microscopy (AFM) in life sciences have been increasing in both variety and significance during the past decade [1–3]. In addition to high resolution imaging of cells, DNA and other biological structures, AFM enables single-molecule mechanics studies characterizing both intramolecular and intermolecular forces [4, 5]. To study biological samples in aqueous environments, which can be corrosive and electrically conducting, we impose challenging electrical isolation requirements. This is especially important for AFM cantilevers or cantilever arrays with integrated piezoelectric detectors or piezoelectric actuators [6, 7]. In order to collect statistically significant data even on a single type of molecule, measurements need to be repeated many times, which requires durable sensors. To implement single-molecule experiments to protein chips for applications such as drug discovery and screening, the throughput needs to be significantly improved. This can be achieved by development of systems that can perform parallel single-molecule measurements on many different molecular pairs [8]. Some parallel techniques have been demonstrated for bond rupture frequency measurements where a molecule of known mechanical properties is used as a force gauge [9]. However, many other single-molecule experiments, such as those that measure bond lifetime at a clamped force, require applying controlled forces on molecules and measuring these forces with piconew-

[4] Present address: Intel Corp., Chandler, AR, USA.

ton resolution. Therefore, both parallel actuation and parallel force sensing are required for parallel single-molecule mechanics experiments. AFM cantilever arrays with integrated piezoelectric actuators and either optical or piezoresistive sensing have demonstrated this capability [6]. These devices, which are used mainly for fast imaging so far, require complex fabrication processes and may be difficult to isolate electrically for operation in liquid environments. Recently, membrane-based probe structures with electrostatic actuation and integrated diffraction-based optical interferometric displacement detection have been introduced for SPM applications [10, 11]. Initial implementation of these force sensing integrated readout and active tip (FIRAT) devices used aluminium membranes over an unsealed air cavity and hence was not suitable for operation in immersion. A version of these surface micromachined structures suitable for operation in biologically relevant, electrically conductive buffer solutions has already been realized for medical ultrasonic imaging applications [12, 13]. These capacitive micromachined ultrasonic transducers (CMUT) use a dielectric material such as silicon nitride as the structural membrane, and a metal actuation electrode buried in the dielectric membrane which is electrically isolated from the immersion medium. The cavity between the membrane and the bottom electrode is sealed under low pressure to prevent liquid leakage [13].

In this paper, we demonstrate in-liquid operation of FIRAT structures for parallel single molecular force spectroscopy and SPM applications. We describe the fabrication procedure of sealed membrane probe arrays on quartz substrates using a low temperature plasma-enhanced chemical vapour deposition (PECVD) dielectric film and a polymer sacrificial layer. We discuss the device characteristics in a liquid environment based on experimental data obtained by the integrated electrostatic actuator and the built-in optical displacement sensor. We also present initial force spectroscopy experiments performed by coupling an AFM cantilever to a functionalized probe membrane in buffer solution. These biomolecular bond unbinding force measurements are performed by pulling the molecules using individually actuated membranes, thereby eliminating the need for the piezoelectric actuator. Therefore, we have demonstrated the feasibility for using these devices in parallel single-molecule mechanics experiments.

2. Structure and operation of micromachined membrane transducer

Figure 1(a) shows a schematic of the membrane-based probe built on top of a quartz substrate. The main structure is a surface micromachined dielectric membrane with a buried metal layer serving as the top electrode. Under the membrane, there is a patterned metal layer (bottom electrode) on top of the substrate. Electrostatic forces actuate the membrane by using the top and the bottom electrodes. The actuation range of the membrane can be controlled with the gap height between the membrane and the substrate as it is typically one-third of the gap. Within this range it is possible to actuate the membrane fast since the speed is only limited by the membrane dynamics.

Optical interferometric displacement detection capability is integrated into the probe by patterning the bottom electrode on the substrate as a diffraction grating. This phase-sensitive

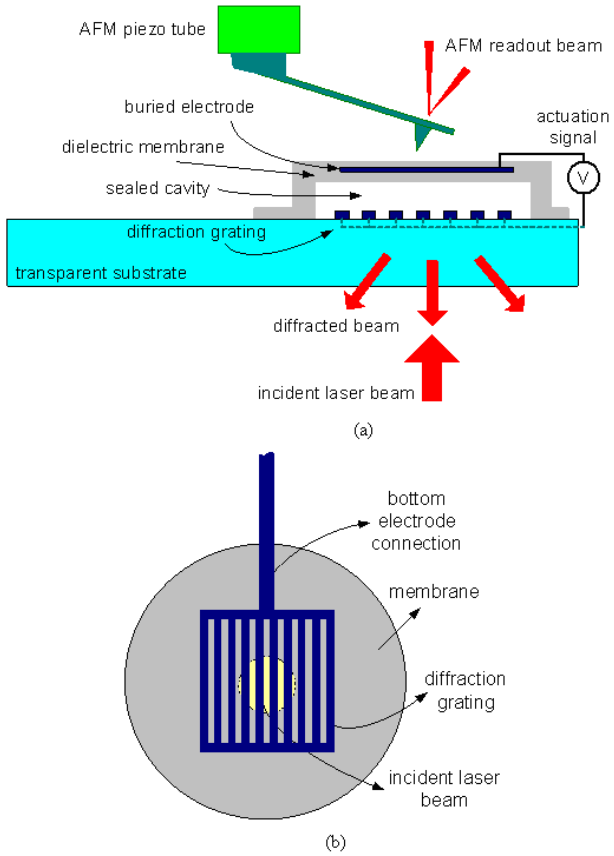

Figure 1. (a) Schematic of the membrane-based probe with integrated electrostatic actuator and integrated optical micro-interferometer with a coupled AFM cantilever in a typical experimental set-up; (b) schematic of an illuminated membrane through the diffraction grating from the backside.

diffraction grating structure enables displacement measurement with the sensitivity of a Michelson interferometer. When the membrane is illuminated from the backside with a coherent light source, the reflected light is separated into diffraction orders as shown in figure 1(a). Moreover, some of the light reflected directly from the diffraction grating interferes with the light reflected from the membrane. Therefore the intensity of light at the diffraction orders varies sinusoidally as a function of the gap between the membrane and the grating. A simple scalar analysis of the reflected light shows that the optical signal in the zeroth order is complementary to the higher diffraction orders [14]:

$$I_0 = I_{\text{in}} \cos^2\left(\frac{2\pi d}{\lambda}\right), \qquad I_{\pm 1} = \frac{4I_{\text{in}}}{\pi^2} \sin^2\left(\frac{2\pi d}{\lambda}\right) \quad (1)$$

where I_{in} and λ are the intensity and wavelength of incident light, respectively, and d is the gap height. Separate photodetectors measure the intensities of the zeroth (I_0) and first ($I_{\pm 1}$) diffraction orders; thus it is possible to implement a differential detection architecture using these photodetector outputs to increase the displacement sensitivity and eliminate the common mode noise components such as laser intensity noise.

An area covering at least four periods of diffraction grating needs to be illuminated to ensure the effective separation of

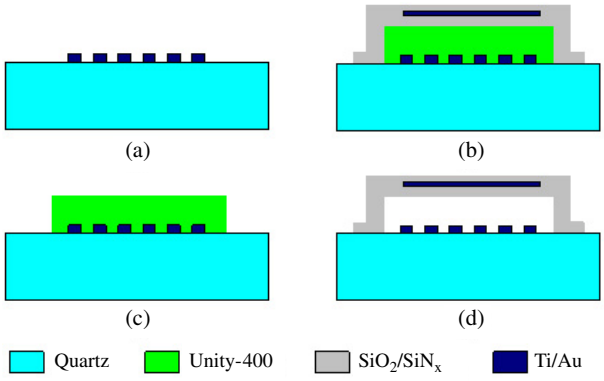

Figure 2. Process flow for the microfabrication of probe membranes.

diffraction orders. Thus the incident beam spot can be reduced to roughly 20 μm in diameter if the minimum width of the fingers forming the diffraction grating is 2 μm. Ideally, the beam spot should be aligned to the centre of the membrane as schematically shown in figure 1(b) since the deflection at the centre is the maximum. To minimize the effect of misalignment of the incident beam the size of the diffraction grating can be made as small as the laser spot illuminating the device so that only the centre portion of the membrane is interrogated. Furthermore, the variation of optical signals as a function of membrane displacement may be calibrated before each experiment using the integrated electrostatic actuator.

Figure 1(a) also shows the typical experimental set-up for a force spectroscopy measurement where a force measuring soft AFM cantilever is coupled to the probe membrane in immersion. Both the cantilever and the membrane are functionalized with appropriate molecular layers. With a relatively stiff membrane, the probe is used as a microscale actuator to bring the tip and the membrane in and out of contact, and the displacement readout can be used to accurately control the extension of the molecules through a feedback loop. With a soft membrane, the probe itself can be used as the force sensor where the membrane displacement due to biomolecular interaction forces is directly detected, eliminating the need for another force sensor such as the AFM cantilever.

3. Fabrication of probe membranes

The microfabrication of the membrane-based probe arrays involves a four-mask process as schematically illustrated in figure 2. Standard IC materials (silicon nitride, silicon oxide, titanium and gold) are used for the mechanical structures whereas a special polymer film (Unity-400) is used as a sacrificial layer in order to increase the gap between the membrane and the substrate without inducing excessive stress on the membranes.

The fabrication process starts with a 500–550 μm thick quartz wafer on top of which 80 nm thick gold diffraction gratings with periods of 3.3, 4.0 and 6.0 μm are formed using e-beam evaporation and a standard lift-off process with the first mask. A 20 nm thick titanium layer is used as an adhesion layer between the gold layer and the substrate.

After the definition of diffraction gratings, the Unity-400 sacrificial polymer [15] is spun at 500 rpm with a ramping speed of 250 rpm for 5 s followed by another spinning at 400 rpm with a ramping speed of 100 rpm for 60 s. After the softbake on a hot plate at 105 °C for 8 min, a flat polymer layer with thickness of 3.2 μm is obtained. Unity-400 is a photo-definable sacrificial polymer, where the exposed area remains (cross-linked). Thus mask #2 is used to pattern the film at the wavelength of 405 nm with an energy density of 60 mJ cm^{-2}. Post-exposure baking takes place in an oven at 125 °C for 15–20 min followed by developing the film in the Avatrel developer. Isopropanol is used to rinse the wafer during the development process. The polymer is then cured inside the Lindbergh furnace at 160 °C for 1 h. After curing, the polymer is thinned down to the thickness of ∼1.9 μm by using O_2 plasma in an RIE chamber.

To define the probe membrane, first a 0.1 μm thick PECVD dielectric layer is deposited on top of the sacrificial layer at 300 °C. The dielectric film consists of Si_3N_4/SiO_2 with a ratio of 0.84:1 to minimize the intrinsic stress built-up in the layer. Then an 80 nm thick gold layer is sputtered to define the top electrode. To promote the adhesion a 5 nm thick titanium layer is used between the gold layer and the dielectric layer to prevent electrical shorting in case the membrane collapses. Mask #3 is used to pattern the Ti/Au layer properly. After metallization another dielectric layer consisting of four sequencing layers of Si_3N_4, SiO_2, Si_3N_4 and SiO_2 with a total thickness of 1.5 μm is deposited. The ratio of Si_3N_4 to SiO_2 is maintained at 0.84:1 as before. The membrane is patterned using RIE etching with mask #4 to form etch holes necessary for the etching of the sacrificial layer.

It is possible to decompose the Unity-400 film by heating up the wafer to a temperature of 440 °C with a furnace that can supply a continuous flow of N_2 gas at 5–10 sccm. Since the membrane is a multi-layered structure, buckling can occur during the decomposition step. Thus, the furnace is heated up very slowly to minimize buckling. Once the sacrificial layer is fully decomposed, the wafer is then diced into chips and the etch holes (see figure 3) are sealed by using epoxy for sealing.

Circular probe membranes with various diameters (50–600 μm) are fabricated. Figure 3(a) shows the photographs of a 600 μm diameter probe membrane. The top view shows the membrane together with one of the etch holes from which the decomposed gas of the Unity-400 film escapes. The bottom view shows the diffraction grating under the membrane through the transparent substrate. Note that this process produces 1D and 2D arrays of membrane-based probes with individual actuation capability. The rightmost photograph of figure 3(a) shows part of the quartz wafer with arrays of probe membranes of different sizes where each column has a different actuation electrode.

The polymer sacrificial layer provides a gap of ∼2 μm as the white light interferometry data shows in figure 3(b). The reflow of the soft polymer layer provides planarization and prevents the translation of the diffraction grating pattern to the membrane as seen from the surface profile. The surface roughness is due to both the definition of the Unity-400 film and the deposition of the dielectric membrane. For biomolecular mechanics measurements, especially when the device is used as an actuator, such as in the force spectroscopy

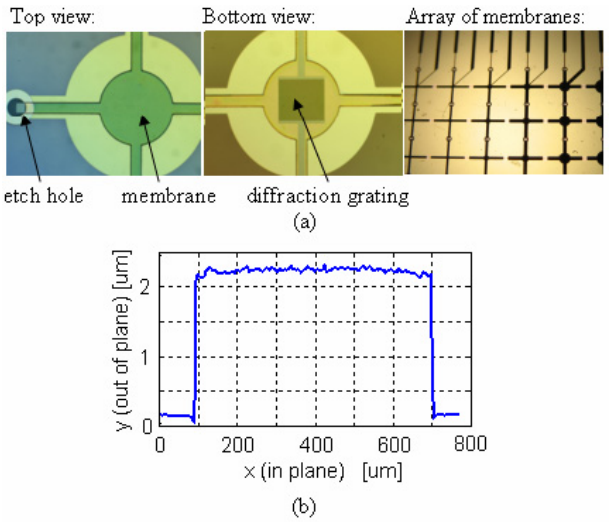

Figure 3. (a) Photographs of a 600 μm diameter probe membrane and an array of membranes with various diameters under a microscope; (b) surface profile of a fabricated membrane obtained using a white light interferometer.

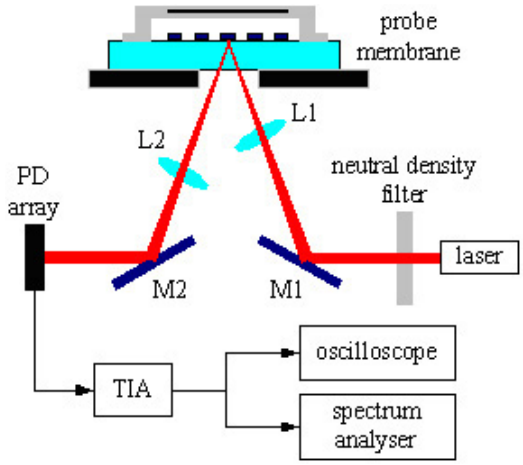

Figure 4. Schematic of the experimental set-up for the characterization of membrane-based probes.

experiments described here, the top surface is flat enough so no further polishing is required since the molecules functionalized on the sharp tip interact locally with the ones on the membrane surface.

For the mechanical characterization, the stiffness of each membrane was measured experimentally using TriboIndenter (Hysitron Inc.), which showed that the stiffness of the fabricated membranes was dominated by residual tensile stress of 30 MPa. Accordingly, the stiffness values of the 100–600 μm membranes are from 600 to 1500 N m^{-1}. Therefore, these membranes are suitable for actuation purposes, where the membrane can be considered rigid as compared to the AFM cantilevers ($k \sim 0.01$–0.05 N m^{-1}) used in the single-molecule mechanics experiments.

The above process is specific for silicon nitride and oxide membrane fabrication. Similar structures can be fabricated using different dielectric membrane materials to achieve desired stiffness values. For example, for higher force resolution, we also fabricated polymer membranes. These membranes are a combination of parylene and metal layers providing lower spring constant values. As a comparison, we measured the spring constant of a 200 μm diameter membrane as 20 N m^{-1} and it is feasible to achieve even softer polymer membranes with a spring constant of 1 N m^{-1}. Details of this process and results will be published elsewhere.

4. Device characterization

To use these active probes in single-molecule mechanics experiments, both the electrostatic actuation and optical interferometric detection capabilities should be well characterized. The electrostatic actuator should provide a suitable actuation range with a reasonable speed whereas the optical interferometer should be capable of resolving as small displacements as possible while providing enough dynamic range. Figure 4 shows the set-up built to characterize the fabricated transducers by applying actuation signals and measuring membrane displacement with the integrated interferometer. The low noise laser module supplies 5 mW laser light at 635 nm. The incident beam passes through a neutral density filter used to adjust laser power incident on the membranes. The beam is then deflected by an adjustable reflective mirror (M1) and focused on the membrane grating with a focusing lens (L1). The beam spot on the diffraction grating plane is approximately 30 μm.

The light intensities in the 0th, +1st and −1st diffraction orders (I_0, I_1, and I_{-1}) are captured and collimated by a lens (L2) before they are directed onto a photodiode (PD) array (Hamamatsu, S4114-46Q) after reflection from a second mirror (M2). The photocurrent (I_{pd}) from the PD array is converted into a readout signal (V_{pd}) by transimpedance amplifiers (TIA) with a gain of 5 kV A^{-1}. The readout signal is fed into an oscilloscope (Tektronix, TDS2004), from which DC and modulated DC signals are monitored, and a dynamic signal analyser (Stanford Research Systems, SR780, Sunnyvale, CA) is used for noise characterization.

For experimental characterization of the actuation performance, a 500 μm diameter transducer membrane with a diffraction grating period of 3.3 μm was used. The membrane was actuated by applying a voltage difference between the electrodes (top electrode and diffraction grating) while monitoring the intensity of light in the diffraction orders by the PD array. Figure 5 shows the measured intensity variations (in terms of voltage, V_{pd}) in the diffraction orders as functions of applied V_{DC}. The intensity of the zeroth and first orders changed periodically as the gap height changed due to the applied voltage, as expected.

The same experiment was repeated under a white light interferometer to measure the membrane displacement as a function of applied bias voltage. Membrane displacement is proportional to the square of voltage and the experiment shows that, for a bias voltage of 50 V, the membrane was displaced by ∼200 nm. Combining these data sets, the optical interference curve (V_{pd}) is mapped to the membrane displacement as shown in figure 6. The interference curve shows a nearly sinusoidal dependence to membrane displacement with a period of 210 nm. The deviation of the curve from the ideal

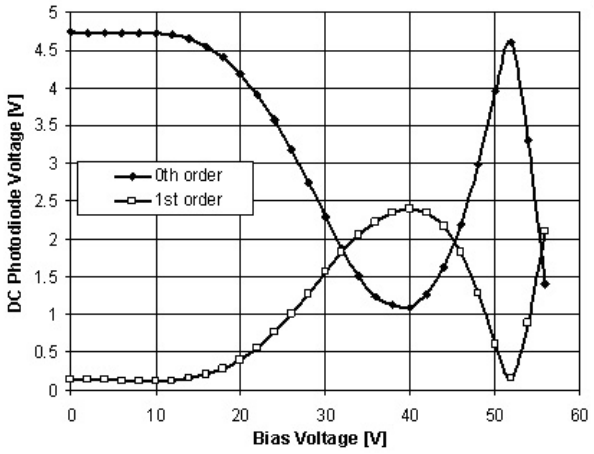

Figure 5. The variation of photodiode output (V_{pd}) with the applied DC bias voltage (V_{DC}) (the membrane was unsealed and in air).

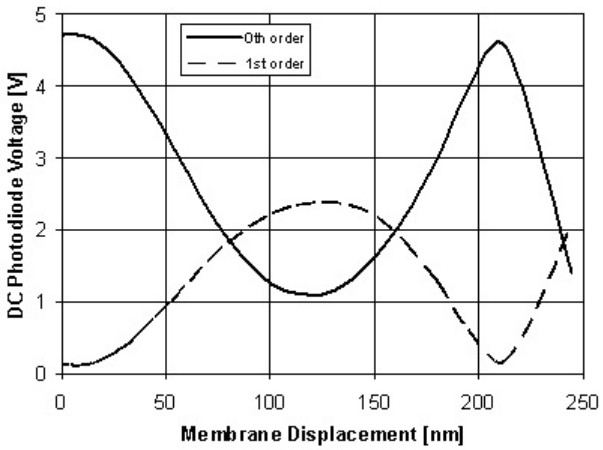

Figure 6. The variation of photodiode output (V_{pd}) with the membrane displacement (the membrane was unsealed and in air).

case can be due to several reasons including the membrane curvature, the angular spectrum of the incident light beam and possible vectorial effects not considered in the scalar formulation used to derive equation (1) [16]. The actuation range for this particular membrane is 580 nm corresponding to approximately 1/3rd of the initial gap of 2 μm, which can be increased for a larger range.

For dynamic characterization, the transducer was excited with a small amplitude AC voltage (V_{AC}) on top of the DC voltage for biasing the probe membrane deflection to the maximum sensitivity point. Sensitivity is defined as the change in V_{pd} divided by the change in membrane displacement.

A 200 μm diameter membrane with sealed etch holes is used for dynamic characterization. The resonant frequency of the membrane in air was 420 kHz, which dropped to 200 kHz when the membrane was operated in buffer solution as shown in figure 7 (the small peak around 30 kHz was due to spurious coupling to the electronics). The flat response of the membrane in liquid up to resonant frequency exceeds the requirements of molecular force spectroscopy as the rupture events usually occur in a few tens of milliseconds [17].

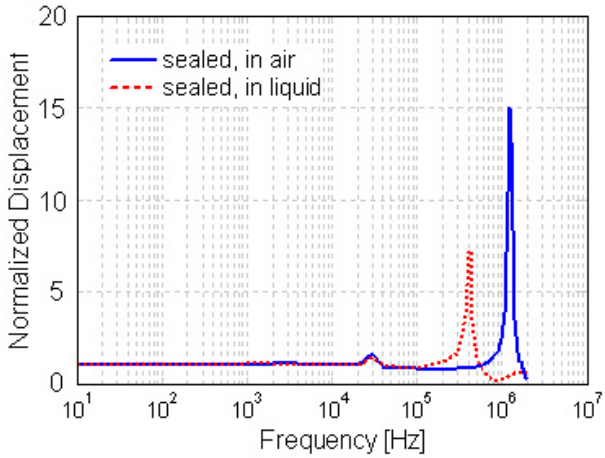

Figure 7. Measured dynamic response of the 200 μm diameter membrane.

The main noise sources in the overall optical detection system that determine minimum detectable displacement (MDD) can be listed as the shot noise in the photodetector, relative intensity noise (RIN) of the laser source, electronic noise of TIA and the thermomechanical noise of the membrane. MDD basically equals the displacement that is measured with a unity signal-to-noise ratio. Figure 8 shows the recorded displacement noise spectral density for a 200 μm diameter membrane. For this experiment, the membrane was biased to its maximum sensitivity point and the noise was read from the PD outputs using a dynamic signal analyser (Stanford Research Systems model # SR785). The differential readout scheme, subtracting the first-order signal from the zeroth-order signal by equating the DC levels, helped suppress the RIN as shown in figure 8 [18]. The displacement noise spectral density floor for the current system was below 10 fm $Hz^{-1/2}$ for frequencies as low as 3 Hz with the differential readout scheme. The noise suppression at the low frequency end (3–1000 Hz) is especially critical since most biomolecular interaction measurements have significant signal components in this range. Overall, more than 20 dB noise suppression is achieved with differential detection. Note that the shot noise in the photodetector for this intensity level was estimated to be $\sim$2.3 fm $Hz^{-1/2}$, and that the theoretical limit was approached for frequencies above 1000 Hz. These measurements show nearly an order of magnitude improvement, especially at low frequencies, as compared to the previously demonstrated interferometric methods [19].

Note that the estimated thermomechanical displacement noise of this membrane in air is well below the shot noise and it is expected to be low even in liquid media because of its large spring constant (1000 N m^{-1}). While the current MDD levels are suitable for actuator feedback, parylene membranes with spring constants of 1–10 N m^{-1} should be used to implement sensors for force spectroscopy experiments, which are currently under investigation.

5. Biological test system and experimental results

We used the interaction between L-selectin and an anti-L-selectin monoclonal antibody (DREG-56) as a biological test

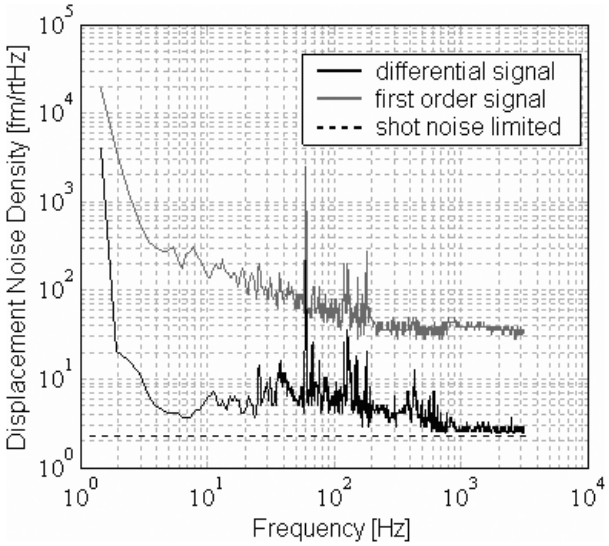

Figure 8. Displacement noise spectrum of the 200 μm diameter probe membrane. The spectrum shows spurious spikes originating from 60 Hz line voltage and mechanical sources which can be eliminated by better shielding and mechanical isolation.

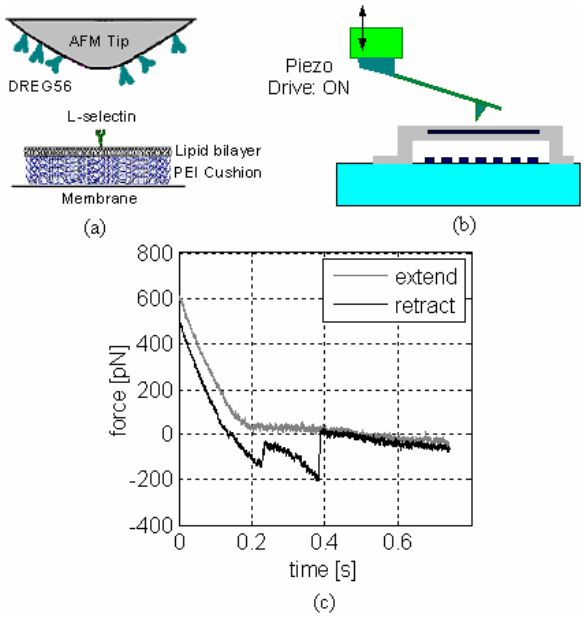

Figure 9. (a) Functionalization of the membrane-based probe and the AFM cantilever with biomolecules; (b) schematic of biological experiment with a stationary membrane and a piezo-actuated AFM cantilever; (c) representative double-break force curve (black trace) obtained during the retract phase experiment. The grey trace is the extend curve.

system for the force spectroscopy experiments. L-selectin is an adhesion molecule on the surface of white blood cells. During inflammatory response, white blood cells use L-selectin to tether to and roll on tissue vasculature [20]. L-selectin reagent is a generous gift from Dr Michael Lawrence (University of Virginia). DREG-56 reagent is a generous gift from Dr R P McEver (Oklahoma Medical Research Foundation). The preparation and characterization of selectin-incorporated polymer-cushioned bilayers formed on glass coverslips have previously been described [17]. In the present study, we used membranes *in lieu* of glass coverslips. Briefly, the membranes were initially coated with a 100 ppm polyethylenimine (PEI) solution (Fisher Scientific, PA) to accommodate the occasionally inversely oriented selectins (figure 9(a)), which proved to be crucial in reducing non-specific adhesion. A 5 μl drop of L-selectin-incorporated lipid vesicle solution was placed on the surface of the probe membrane, incubated for 15–20 min under a wet paper towel and covered with Dulbeccos phosphate buffered saline (DPBS) solution (Fisher Scientific, PA) containing Ca^{2+}, Mg^{2+} and 1% bovine serum albumin (BSA). The bilayers so formed have low molecular densities, which ensures their infrequent binding (30–40% double-check this) to the mAb-coated cantilever tips, a condition necessary to ensure that the majority of the events would be single instead of multiple molecular interactions. The bilayers were immediately used in the experiments. DREG-56 was directly adsorbed on the cantilever tip [17].

Initial experiments were performed by repeatedly moving the AFM tip with the piezo-actuator of the commercial AFM system while a 200 μm diameter probe membrane was kept stationary as shown in figure 9(b). The interaction forces were detected from the optical lever detection mechanism of the AFM system. Figure 9(c) shows a typical force curve with a double break with rupture forces comparable to previously published data [17]. Upon testing, the adhesion frequency (i.e. the fraction of binding events) was ~40%, consistent for several different membrane–tip pairs, thus demonstrating repeatability and reproducibility of our biological protocol. In order to clearly demonstrate the specificity of the observed interactions, a control experiment was performed wherein the L-selectin in the bilayer was blocked using excess DREG-56. Upon blocking, the adhesion frequency dropped dramatically to 6%, on par with nonspecific adhesion levels. This suggests that an intact bilayer with reconstituted L-selectin was formed on the surface of the membrane probe, which not only supported specific L-selectin interaction with DREG-56 but also presented a small fraction of nonspecific interactions. The majority of the binding events exhibited only single breaks, with progressively smaller numbers of binding events that showed double as well as triple breaks, which is consistent with a Poisson distribution and suggests that each break represents unbinding of a single L-selectin-DREG-56 bond.

In subsequent experiments, the piezo-actuation was disabled and the probe membrane was actuated using the built-in actuator as sketched in figure 10(a). To test the actuator under liquid, the AFM cantilever was pressed on the membrane, which was driven with a 5 V peak triangular wave at 5 Hz. Since the piezo-actuator was turned off, the cantilever bending should be caused by the membrane deflection, which is proportional to the square of the actuation signal, shown in figure 10(b). In support of this contention, the measured force–time course ramped up for about 0.05 s and then ramped down as shown in figure 10(c), concurrent with the time course of the voltage applied to drive the membrane. Then the AFM cantilever was lifted slightly so that the membrane movement would bring it in and out of contact with the cantilever. The experiment was repeated to detect the possible rupture events.

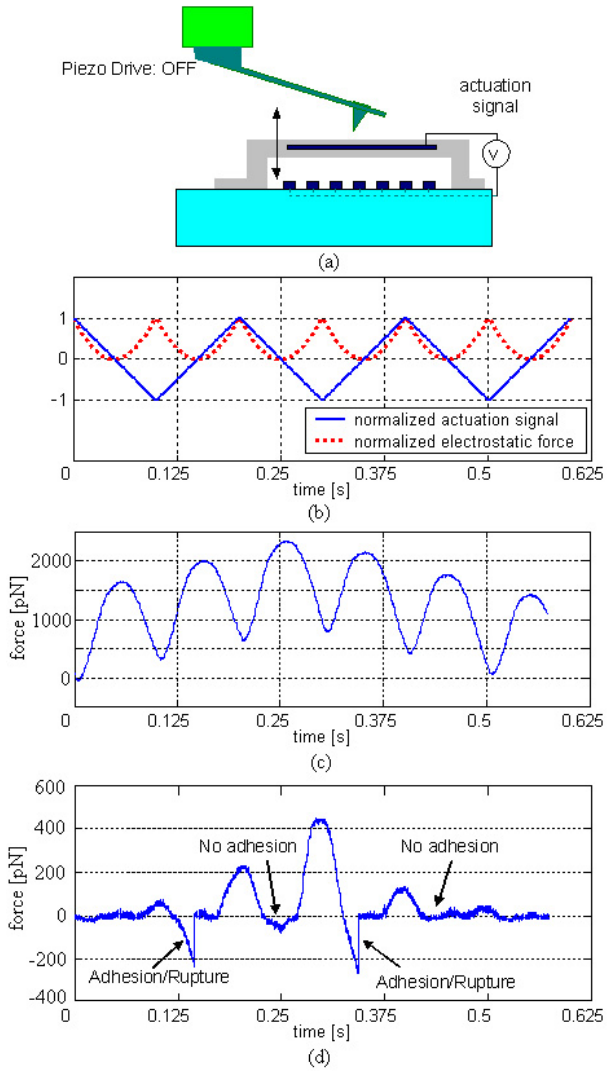

Figure 10. (a) Schematic of biological experiment with electrostatically actuated active probe membrane and disabled piezo-drive for the cantilever; (b) the actuation signal applied to the probe membrane and the generated electrostatic force, which is proportional to the square of the actuation signal; (c) the cantilever and the probe membrane were in full contact and moved together; (d) the detected rupture events as the probe membrane was actuated into and out of contact with the AFM cantilever.

Figure 10(d) shows a typical force curve so obtained. Initially the cantilever and the membrane were out of contact so the cantilever force remained zero as the membrane moved up. When the membrane made contact with the cantilever, the compressive force increased accordingly, i.e. when the slope of the curve is positive. Then the membrane moved down together with the cantilever with a negative slope on the force curve. Before the membrane moved out of contact from the cantilever, a clear adhesion event was detected. The cyclic operation went on in this manner and a total of two rupture events were detected out of four for the force–time curve shown in figure 10(d). The observed unbinding forces are in agreement with the previous experiment in which the piezo-drive was active and the membrane was stationary, as shown in figure 9(c).

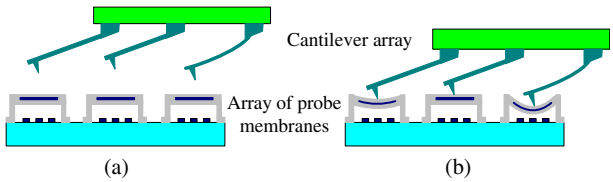

Figure 11. (a) Schematic of an array of individually actuated membrane transducers used as a locally actuated sample surface under a stationary AFM cantilever array. (b) It is possible for individually actuated transducer membranes to conform to the AFM cantilevers after engagement to compensate possible non-uniformities.

6. Discussion

The experimental results presented show that micromachined probe membranes can be individually actuated for single-molecule force spectroscopy measurements. Furthermore, arrays of these membranes have already been fabricated as shown in figure 3(a). A natural extension of this approach shows a path to parallel force measurements where individually actuated membranes are used to conform to stationary cantilever arrays as shown schematically in figure 11. With this method, the force exerted by the cantilever tips on the molecules under investigation can be precisely controlled. Note that, in this configuration the molecular interaction forces are still measured using the AFM cantilevers, but since the pulling motion is provided by the individual active probe membranes, the cantilevers do not have to be individually actuated, thus eliminating a significant bottleneck for single molecular assays. Since the membranes in the array configuration are individually actuated, it is possible to electrostatically bias the membranes to compensate possible fabrication non-uniformities across the membrane actuator array. An acceptable level of non-uniformities in an array configuration has already been demonstrated and characterized using CMUT array structures [13].

Non-cantilever based parallel force spectroscopy is also possible using these membrane based probes both as actuators and force sensors. The experiments can be performed by integrating sharp tips to the probe membranes as in the case of FIRAT and designing membranes with proper stiffness [11]. Moving these functionalized sharp tips against a stationary substrate may eliminate the need for microcantilevers. Note that for parallel readout of cantilever arrays by optical levers as in figure 11, one needs to adjust both the angle and location of each readout beam to compensate for the curvature of each cantilever in the array. In contrast, only lateral alignment of the array chip is needed for FIRAT based arrays with interferometric detection. Since the reflected diffraction order locations are pre-determined by gratings on a rigid substrate geometry, one does not need to move the laser beams or the photodetector arrays. Therefore, the complexity of the optical design can be expected to be at the same order as optical lever arrays, which have already been realized. Then, each soft membrane would provide force detection with high sensitivity as a force sensor. As discussed in section 3, polymer membranes have already been fabricated with a spring constant of a few tens of $\mathrm{N\,m^{-1}}$. Using carefully

designed micromachined mechanical structures with spring constants in the 1 N m^{-1} range and noise levels down to 10 fm Hz$^{-1/2}$, one can achieve pN force resolution with 10 kHz measurement bandwidth with this device. We also note that the membrane structures presented here can be designed to have actuation bandwidths larger than 100 kHz as seen in figure 7, far exceeding the range of typical piezoelectric tubes. If the sample structures with small mass loading such as biomolecular layers are immobilized on these membranes, these structures can also be used as microscale actuators for fast AFM imaging in fluids.

Acknowledgments

We thank Guclu Onaran and Fang Kong for their help with the experimental set-up. The National Institutes of Health (Grant No. R01 AI060799) provided the financial support for this research.

References

[1] Fotiadis D, Scheuring S, Muller S A, Engel A and Muller D J 2002 Imaging and manipulation of biological structures with the AFM *Micron* **33** 385–97
[2] Shao Z F, Mou J, Czajkowsky D M, Yang J and Yuan J Y 1996 Biological atomic force microscopy: what is achieved and what is needed *Adv. Phys.* **45** 1–86
[3] Yang J and Shao Z F 1995 Recent advances in biological atomic-force microscopy *Micron* **26** 35–49
[4] Rief M and Grubmuller H 2002 Force spectroscopy of single biomolecules *ChemPhysChem* **3** 255–61
[5] Zlatanova J, Lindsay S M and Leuba S H 2000 Single molecule force spectroscopy in biology using the atomic force microscope *Prog. Biophys. Mol. Biol.* **74** 37–61
[6] Sulchek T, Grow R J, Yaralioglu G G, Minne S C, Quate C F, Manalis S R, Kiraz A, Aydine A and Atalar A 2001 Parallel atomic force microscopy with optical interferometric detection *Appl. Phys. Lett.* **78** 1787–9
[7] Vettiger P *et al* 2002 The 'millipede'—nanotechnology entering data storage *IEEE Trans. Nanotechnol.* **1** 39–55
[8] Albrecht C H, Clausen-Schaumann H and Gaub H E 2006 Differential analysis of biomolecular rupture forces *J. Phys.: Condens. Matter* **18** S581–99
[9] Blank K *et al* 2003 A force-based protein biochip *Proc. Natl Acad. Sci. USA* **100** 11356–60
[10] Degertekin F L, Onaran A G, Balantekin M, Lee W, Hall N A and Quate C F 2005 Sensor for direct measurement of interaction forces in probe microscopy *Appl. Phys. Lett.* **87** 213109
[11] Onaran A G, Balantekin M, Lee W, Hughes W L, Buchine B A, Guldiken R O, Parlak Z, Quate C F and Degertekin F L 2006 A new atomic force microscope probe with force sensing integrated readout and active tip *Rev. Sci. Instrum.* **77** 023501
[12] Jin X C, Ladabaum I, Degertekin F L, Calmes S and Khuri-Yakub B T 1999 Fabrication and characterization of surface micromachined capacitive ultrasonic immersion transducers *J. Microelectromech. Syst.* **8** 100–14
[13] Knight J, Mclean J and Degertekin F L 2004 Low temperature fabrication of immersion capacitive micromachined ultrasonic transducers on silicon and dielectric substrates *IEEE Trans. Ultrason. Ferroelectr. Freq. Control* **51** 1324–33
[14] Hall N A and Degertekin F L 2002 Integrated optical interferometric detection method for micromachined capacitive acoustic transducers *Appl. Phys. Lett.* **80** 3859–61
[15] Reed H A, White C E, Rao V, Allen S a B, Henderson C L and Kohl P A 2001 Fabrication of microchannels using polycarbonates as sacrificial materials *J. Micromech. Microeng.* **11** 733–7
[16] Lee W and Degertekin F L 2004 Rigorous coupled-wave analysis of multilayered grating structures *J. Lightwave Technol.* **22** 2359
[17] Sarangapani K K, Yago T, Klopocki a G, Lawrence M B, Fieger C B, Rosen S D, Mcever R P and Zhu C 2004 Low force decelerates L-selectin dissociation from P-selectin glycoprotein ligand-1 and endoglycan *J. Biol. Chem.* **279** 2291–8
[18] Hobbs P C D 1997 Ultrasensitive laser measurements without tears *Appl. Opt.* **36** 903–20
[19] Manalis S R, Minne S C, Atalar A and Quate C F 1996 Interdigital cantilevers for atomic force microscopy *Appl. Phys. Lett.* **69** 3944–6
[20] Mcever R P 1991 Selectins—novel receptors that mediate leukocyte adhesion during inflammation *Thromb. Haemost.* **65** 223–8